European Journal of Mechanics B/Fluids 29 (2010) 201–207

Contents lists available at ScienceDirect

European Journal of Mechanics B/Fluids

journal homepage: www.elsevier.com/locate/ejmflu

Influence of coaxial cylinders on the vortex breakdown in a closed flow

C. Cabeza [a], Gustavo Sarasúa [a], Arturo C. Martí [a,*], Italo Bove [a], Sylvana Varela [a,b], Gabriel Usera [b,c], Anton Vernet [b]

[a] Instituto de Física, Universidad de la República, Montevideo, Uruguay

[b] Departament d'Enginyeria Mecánica, Universitat Rovira i Virgili, Tarragona, Spain

[c] Instituto de Mecánica de los Fluidos, Facultad de Ingeniería, Universidad de la República, Montevideo, Uruguay

ARTICLE INFO

Article history:
Received 25 November 2008
Received in revised form
12 November 2009
Accepted 27 January 2010
Available online 6 February 2010

Keywords:
Vortex breakdown
Recirculation flow
Control

ABSTRACT

The effect of stationary cylindrical rods located at the centerline axis on the vortex breakdown (VB) in a closed flow is studied experimentally and numerically. The flow takes place in a cylindrical container with a rotating end wall. The dimensionless numbers characterizing the dynamics of the system are the Reynolds number, based on the angular velocity of the rotating wall, the aspect ratio of the container and dimensionless radius of the rod. We find that the onset of VB, as a function of the Reynolds number, is anticipated for very small values of the rod radius R_r, while it is delayed for values of R_r beyond a critical value. In order to characterize this effect, the critical Reynolds number for the appearance of the vortex breakdown as a function of the radius of the stationary rods and the different aspect ratios was accurately determined, using digital particle image velocimetry and numerically using a three-dimensional Navier–Stokes solver. The numerical and experimental results are compared showing an excellent agreement.

1. Introduction

The development of structural changes in vortical flows and, particularly, vortex breakdown [1–5] has been intensively investigated during the past few years [6–19]. The characteristic and fundamental signature of the vortex breakdown is the appearance of a stagnation point followed by regions of reversed axial flows with a bubble structure when the swirl is large enough. This structural change is also accompanied by a sudden change of the size of the core and the appearance of disturbances downstream the enlargement of the core. The vortex breakdown is very important in several applications of fluid mechanics such as aerodynamics, combustion, nuclear fusion reactors or bioreactors. The presence of this phenomenon in these devices may be beneficial or detrimental, depending on each particular application [13,14].

The vortex breakdown (VB) has been firstly observed in open flows [1], but subsequently it has also been obtained in experiments performed in confined flows, for example, in closed cylinders [5]. It is worth noting that the characteristics of VB in both cases are strongly similar, suggesting the possibility that the basic mechanism of VB is the same in both situations [10]. Experimental measurements show that flows in open channels can be accurately described with the relatively simple q-vortex model [4]. On the other hand, an analytical description for open flows which are considerably more complex than closed flows is not known [5–7]. Thus, experiments performed with flows confined in cylinders are very attractive in order to understand the basic mechanism of VB, as well as to investigate possible control mechanisms.

Due to the great number of practical implications of VB, the development of mechanisms for controlling its emergence is of considerable interest. Recently, different methods for controlling VB in closed flows have been proposed using different techniques. The effect of adding a small, rotating or stationary, cylinder at the axis of the container was first investigated using numerical and experimental techniques, by Mullin et al. [11]. They found that sloping the inner wall has a dramatic effect on the recirculation. More recently, Husain et al. [13] considered the addition of co- or counter-rotation near the axis using a small central rod rotating independently of the bottom or rotating end wall. They concluded that such method may be an effective way to either enhance or suppress VB.

Other approaches are based on the introduction of a small rotating disk in the end wall opposite to the rotating wall [14,20,21], or the use of axial temperature gradients [22]. More recently, Lo Jacono et al. [23] studied the effect of the length of the rod. They found that for long axial, coincidently with the other previous results, rods the co-rotation suppresses VB, unlike counter-rotation which enhances the VB region. For short rod length, the behavior of the recirculation zone is more complex and as the rods shorten the behavior approaches the limit of a flat disk and the recirculation zone bubble vanishes for sufficient counter-rotation speed.

* Corresponding author. Tel.: +598 25258624; fax: +598 25250580.
E-mail address: arturomarti@gmail.com (A.C. Martí).

0997-7546/$ – see front matter © 2010 Elsevier Masson SAS. All rights reserved.
doi:10.1016/j.euromechflu.2010.01.003

Mullin et al. [11] found that a straight small cylinder does not change qualitatively the characteristics of the flow. Specifically, they considered the case of a stationary cylinder for the fixed aspect ratio and the Reynolds number and they did not find important qualitative changes with respect to the case without an inner cylinder. They concluded that it is necessary to slope the inner boundary in order to significantly alter the VB bubble. However, as these authors recognize, it is difficult to find a reliable measure for the onset of VB with the technique employed in their work, i.e. dye visualization. It is clear that a more accurate technique is necessary in order to get quantitative experimental results for the VB onset.

Although the previously mentioned techniques refer to steady VB, it is also worth noting that for large enough *Re* numbers, VB can be time dependent. In a recent paper, Lopez et al. [24] present numerical and experimental results concerning the control of *unsteady* VB in confined cylindrical flows. The control is achieved by modulating with low amplitudes the frequency of the rotating disk. It is found that the oscillations of the VB bubble can be enhanced for low modulation frequencies, or, suppressed for higher frequencies.

The aim of this work is to analyze accurately the effect of the presence of a rod at the cylinder axis on the onset of VB for a range of important parameters. Since the onset of VB is associated with the appearance of a stagnation point near the axis an accurate determination of the velocity field is necessary. Digital particle image velocimetry (DPIV) technique is used to obtain the critical Reynolds number for the onset of VB as a function of the aspect ratio and radius of the inner cylinder. In order to gain a deeper understanding of the internal structure of the flow and accuracy in the critical Reynolds numbers, we considered necessary to complement our experimental observations with numerical simulations. It is found that the existence of rods can affect significantly the critical value of the Reynolds number, Re_c for the onset of VB.

This paper is organized as follows. First, in Section 2 we present the experimental setup and general observations about the onset of VB. In Section 3, we describe the numerical method used in the simulations. The comparison between the experiments and the numerical calculations is given in Section 4. Finally, in Section 5, we present a summary and the conclusion.

2. Experimental setup

The experimental setup consists of a Plexiglas cylindrical container of inner radius $R = 40.0$ mm, a rotating disk at the top and a stationary disk at the bottom of the cylinder (see Fig. 1). The rotating disk is driven by an electronically controlled DC motor, operating with angular velocity between $\omega_0 = 1$ rad/s and $\omega_0 = 21$ rad/s, with an error of less than 0.5% in the measurement of ω_0. The height of the flow domain, H, and therefore the aspect ratio H/R, can be varied by moving the rotating disk up and down to a predetermined location. In this work, three different aspect ratios H/R: 1.5, 2 and 2.5 were considered.

In a first series of experiments, the emergence of vortex breakdown in the absence of the rod for comparison with results of previous works is analyzed. In the second part, the effect of axial rods on VB development is investigated. We use the cylindrical container described above, with an axial stationary rod fixed on the bottom disk. The rod was perfectly aligned along the axis of the container and was kept at rest during the experience. Three different rod sizes, with corresponding radius $R_r = 1.0$ mm, $R_r = 2.5$ mm and $R_r = 5.0$ mm were used ($R_r/R = 0.025$, $R_r/R = 0.0625$, and $R_r/R = 0.125$ respectively).

The fluid used was water dissolutions of glycerin at 60% in mass, with kinematics viscosity $\nu = 1.0 \times 10^{-5}$ m^2/s. Neutrally buoyant polyamide particles of 50×10^{-6} m diameter were seeded inside the fluid in order to obtain the velocity profile. A vertical green laser sheet of 100 mW, with 2 mm of width was used as the illumination

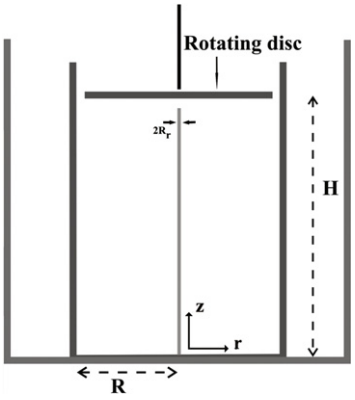

Fig. 1. The experimental setup consists of a closed cylinder, radius R and height H, with a rotating top wall. Along the axis of the cylinder a stationary rod of radius R_r is located. An external container was used in order to minimize the optical distortion of the images due to the curvature of the cylindrical wall.

system. The sheet was focalized at the meridional plane of the cylinder. The images of the flow were recorded using a PIXELINK PL-A741 CMOS camera at 80 frames per second corresponding to 608×608 pixels window size. In order to eliminate shadows and interferences effects in the images due to the curvature of the cylindrical wall, the container was immersed in a rectangular box filled with the same working fluid, since both the solution and the Plexiglas have similar refractive indexes.

The onset of VB is typically associated with localized regions of reverse flows, i.e. an internal stagnation point on the vortex axis appears, located at a certain height, z_c. The appearance of VB bubbles is a manifestation of internal separation of the streamlines from the axis, causing the reversal of the axial velocity. We used the criteria that VB arises when the axial velocity changes the sign at the axis. In the situation when a stationary rod is localized at the axis of the cylinder, we analyze the vertical velocity very close to the rod. Experimentally axial velocity profiles were obtained at 1 mm of rods wall; this length corresponds to one pixel in images with zoom. Numerically, the axial velocity profile shown corresponds to the estimate in the first cell, locate a 0.01 cm from the rods wall for all aspect ratios. In the case of the cylinder without rod, axial velocity profiles were estimate at the axis.

In order to obtain the velocity field inside the flow, the conventional digital particle image velocimetry (DPIV) (see for example [25,26]) technique was implemented. This technique allows us to get accurate quantitative values of the velocity profiles based on the cross-correlation of two consecutive images. In fact, this technique also allows us to determinate accurately the critical Reynolds number, Re_c, at the onset of VB through the measurement of the vertical velocity at the axis of the cylinder.

Fig. 2 shows the typical DPIV images and their respective velocity field for the onset of VB corresponding to different configuration for $H/R = 2$. These images were analyzed using the Matlab tool based on correlations URAPIV with a 64×64 pixels interrogation window and 16 pixels overlapping. The experiments were conducted in an air-conditioned room at 20 °C and the fluid temperature was monitored regularly using a thermocouple located at the bottom of the external container. The Reynolds number was defined as in previous works as $Re = \omega_0 R^2/\nu$, which varies in the experiments between 600 and 2900, with a 2% of error.

In Fig. 3 three typical axial velocity profiles at the axis ($r = 0$) for $H/R = 2$ corresponding to the cylinder without rod are shown. In Fig. 3(a), previous to the onset of VB, the axial velocity is always positive and in this case the Reynolds number is $Re = 1391$. At the onset of VB, Fig. 3(b) corresponding to $Re_c = 1474$, the axial velocity present a null value at the stagnation point located at $z_c/R = 0.78$ above the bottom of the cylinder. Finally, in Fig. 3(c),

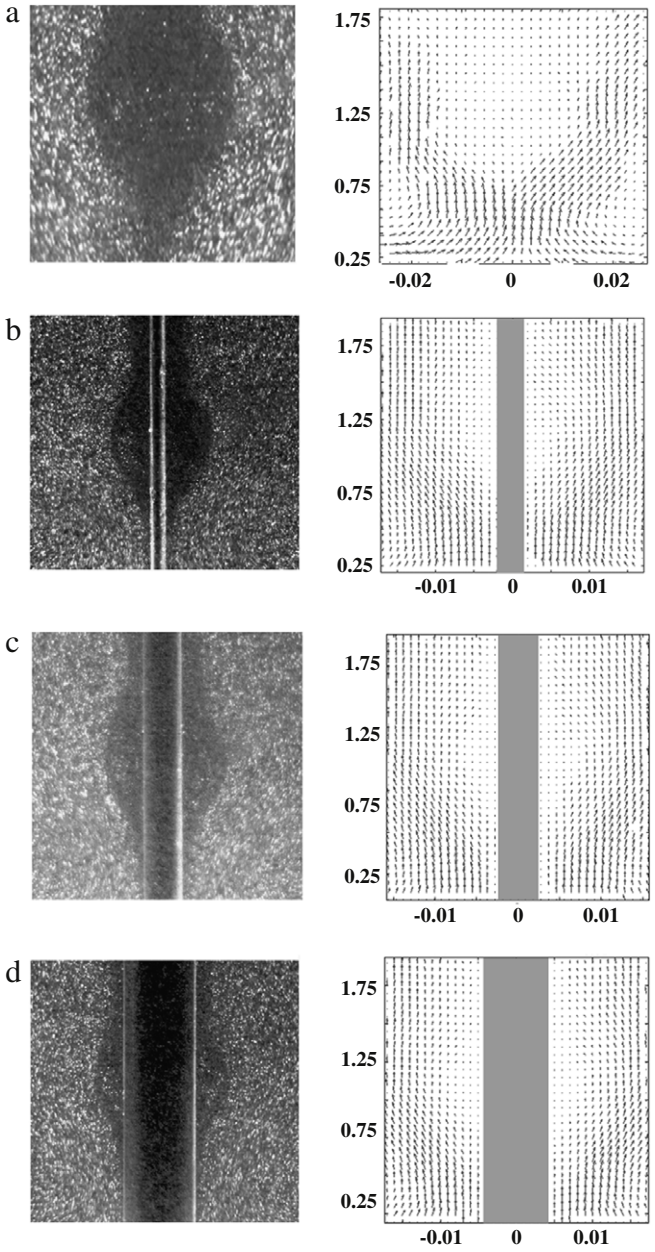

Fig. 2. PIV images and velocity fields of the region in which the recirculation bubble is located at the onset of VB for different radius of the rod. The aspect ratio ($H/R = 2$) is the same in all the images while the Re_c varies in each image: (a) $Re = 1474$, without rod; (b) $Re = 1313$, $R_r/R = 0.025$; (c) $Re = 1431$, $R_r/R = 0.0625$; (d) $Re = 1671$, $R_r/R = 0.125$.

we can observe that the second VB takes place at $Re_c = 1836$. In this case, the axial velocity at the axis presents a range of negative values in the place of the first recirculation bubble and a second stagnation point at $z_c/R = 1.13$ above the bottom of the cylinder.

3. Numerical method

The numerical simulations considered here were obtained with the in-house flow solver caffa3d.MB developed jointly by Universitat Rovira i Virgili (Tarragona, Spain) and Universidad de la República (Montevideo, Uruguay). It is an original Fortran95 implementation of a fully implicit finite volume method for solving the 3D incompressible Navier–Stokes equations in complex geometry, using block-structured body-fitted grids. This three-dimensional solver is based on a two-dimensional solver described in [27]. Further description of this model can be found in Refs. [28–30]. Remarkably, in Ref. [30] the code is shown to accomplish second-order convergence both in space and time.

The mathematical model comprises the mass, Eq. (1), and momentum, Eq. (2), balance equations for an incompressible Newtonian fluid

$$\int_S \left(\vec{\boldsymbol{v}} \cdot \hat{\boldsymbol{n}}_S\right) \mathrm{d}S = 0 \tag{1}$$

$$\int_\Omega \rho \frac{\partial u}{\partial t} \mathrm{d}\Omega + \int_S \rho u \left(\vec{\boldsymbol{v}} \cdot \hat{\boldsymbol{n}}_S\right) \mathrm{d}S = \int_S -p\hat{\boldsymbol{n}}_S \cdot \hat{\boldsymbol{e}}_1 \mathrm{d}S + \int_S \left(2\mu \boldsymbol{D} \cdot \hat{\boldsymbol{n}}_S\right) \cdot \hat{\boldsymbol{e}}_1 \mathrm{d}S. \tag{2}$$

These equations hold in any portion Ω of the domain, S being the boundary of Ω and $\hat{\boldsymbol{n}}_S$ the outward normal vector at the boundary S. The momentum balance equation (2) is expressed for the first Cartesian component u of the velocity vector $\vec{\boldsymbol{v}} = (u, v, w)$, with similar expressions holding for the other components. The dynamic viscosity μ of the fluid and the symmetric deformation tensor $\boldsymbol{D}$ were used for the viscous term.

Since the Reynolds number was relatively low for all cases, namely, from $Re = 800$ to $Re = 2700$, no turbulence model was required so transient solutions were directly computed. The time step was set to 10^{-1} s for all cases. Simulations were run starting from null velocity fields through 10^3 time steps, or about 100 s of flow time. To determine an appropriate grid resolution for grid-independent results, simulations were performed for three different resolution levels. We work with grids of $72 \times 40 \times 100$ (low resolution), $108 \times 60 \times 150$ (mid resolution) and $144 \times 80 \times 200$ (high resolution) cells.

Two different grid topologies were used, one to study the fluid without rods, and the other to study the system including rods. The different choices for these two cases reflect that a boundary condition near the axis exists for the case that includes rods, while no boundary condition exists at the axis for the case without rods. In the first case, the grid used for the cylinder without rods is a block-structured grid, made of two blocks. The inner one is a prism of a square base of 5 mm (0.2592×10^6 cells) located in the axis of the cylinder, while the outer one is a C-grid block that wraps around the first one, see Fig. 4(a) (2.304×10^6 cells). Thus, the two-block grid strategy adopted for the first case ensures that the critical region near the axis is treated entirely as an inner region in the absence of a rod, not requiring the specification of delicate boundary conditions there. Concerning the second case, corresponding to the system with rod, a C-grid block, with a no-slip boundary condition at walls, Fig. 4(b), is used. This single cylindrical block is the natural choice allowing a direct specification of the non-slip boundary condition at the rod.

As mentioned before, in order to check the effect of grid resolution on the numerical results, simulations were performed for three different resolution levels. Fig. 5 illustrates the numerical results for the three grid resolutions tested, more specifically it shows axial velocity profiles at the first cell from the wall of the rod. The fine grid resolution was selected for all simulations. The convergence trend with respect to spatial resolution in Fig. 5 is consistent with the second-order convergence rate of the solver reported in Ref. [28] and suggests that no further grid refinement is necessary. Furthermore, for high Re values numerical results for the fine grid resolution have differences less than 5% with respect to experimental results obtained by Escudier [5]. Among other factors, high resolution simulations are less affected by numerical diffusion, approaching the correct behavior for given Re values.

The numerical model allows us to get the three cylindrical components of the velocity field (v_r, v_θ, v_z) and its derivatives. As mentioned before, the reversals of the axial component of the

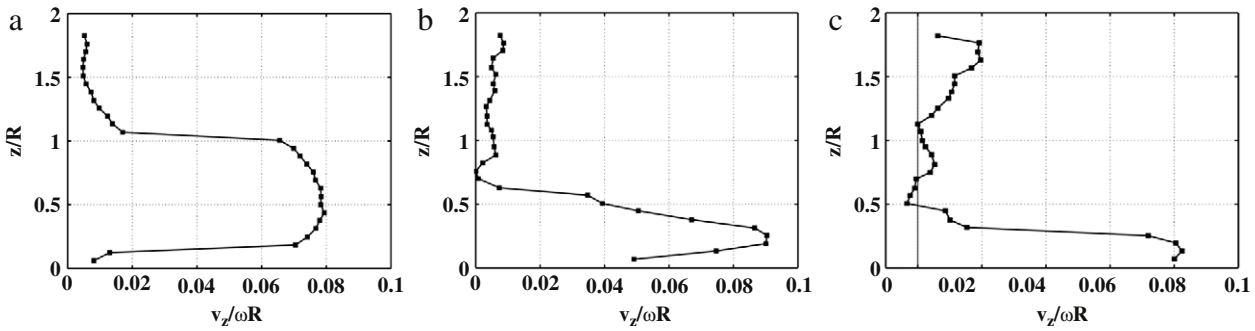

Fig. 3. Axial velocity profiles at the axis ($r = 0$) for $H/R = 2$ obtained using the DPIV technique and corresponding to the cylinder without rod. (a) Situation before the onset of VB, $Re = 1391$, the axial velocity at the axis is always positive. (b) First VB, $Re = 1474$, the axial velocity at the axis present a null value at the stagnation point located at $z_c/R = 0.78$. (c) Onset of the second VB, $Re = 1836$, in this case the axial velocity at the axis presents a range of negative values in the place of the first recirculation bubble and a second stagnation point at $z_c/R = 1.13$ where the second bubble is going to appear.

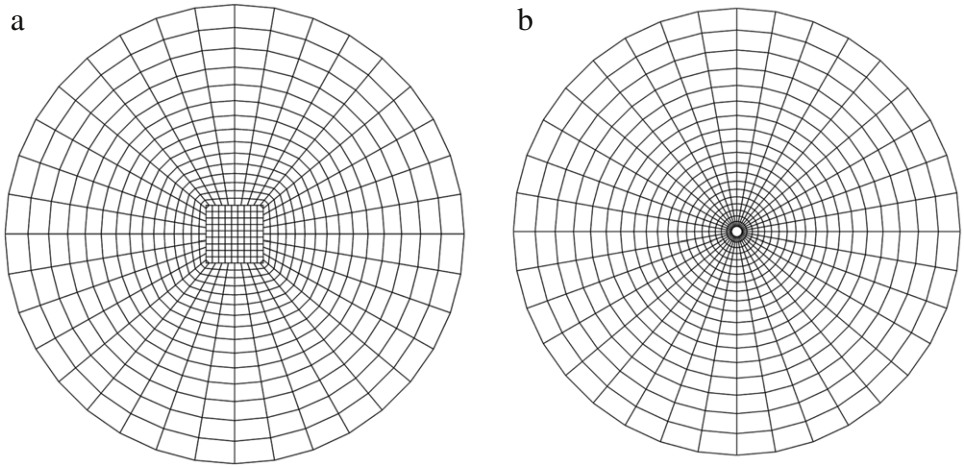

Fig. 4. (a) Cross section of the block-structured grid, with a central square block, used in the case of the cylinder without rod. This grid topology prevents the need for internal boundary conditions at the axis of the domain for the case without rod. (b) Cross section of the structured grid for the case of the cylinder with a rod.

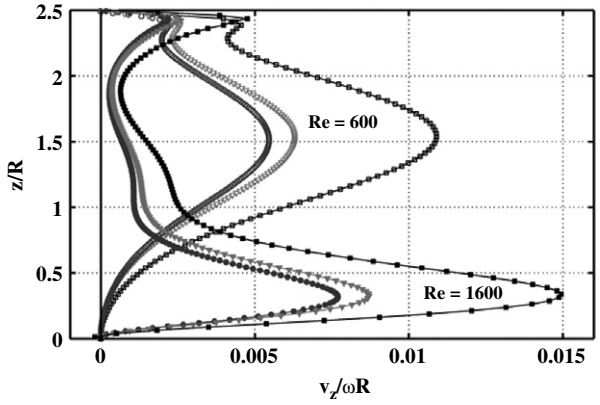

Fig. 5. Axial velocity profiles at the first cell from the wall of the rod for the three different grid resolutions tested (without rod, aspect ratio $H/R = 2.5$ radius of the rod). The symbols correspond to $Re = 600$ (empty symbols) and $Re = 1600$ (full symbols) in high (circle), mid (triangle) and low (square) resolution.

velocity v_z in the region near the axis gives us information on the emergence of areas of recirculation (bubbles), which are a way of determining VB. In Fig. 6 numerical results of the axial component of the velocity are shown for the cylinder without rod. The two showed panels correspond to one (top) and two (bottom) VB bubbles. This velocity profiles show an excellent agreement with those obtained experimentally shown in Fig. 3.

The simulations are performed for different cases (three values of the aspect ratio H/R, cylinder with and without rods) and Reynolds numbers. The numerical results are in excellent agreement with the experimental velocity profiles. The position of the stagnation point is obtained with a difference less than 5% in the system with and without rods. The numerical results were analyzed trough streamlines ψ and azimuthal vorticity $\eta_\theta = \eta_y \cos\theta - \eta_x \sin\theta$.

Fig. 8 shows contours for the azimuthal vorticity η_θ in the meridional plane for $H/R = 2$ at critical Reynolds number Re_c as indicated. The contour levels are non-uniformly spaced, with 20 levels in the positive range and 20 in the negative one determined by $level_{pos}(i) = Max(variable) \times (\frac{i}{20})^3$ and $level_{neg}(i) = Min(variable) \times (\frac{i}{20})^3$ [6]. All the fields are plotted at $t = 100$ s, when steady-state flow conditions have been reached.

4. Results and discussion

In order to validate and compare our work with previous studies [5], the emergence of the vortex breakdown in the absence of rods has been analyzed. Table 1 shows the numerical and experimental results obtained in the present work with the results reported by Escudier [5]. It can be observed that the results obtained from the experimental DPIV analysis and those obtained by the numerical simulation show an excellent agreement with differences lower than 2%. On the other hand, the differences between our results and those described by Escudier [5] show differences smaller than 3%. Thus, it can be concluded that the experimental and numerical methods used in the present work are very reliable. Now, we consider the situation in which an axial stationary rod of radius R_r is present. Table 2 shows the critical Reynolds number obtained

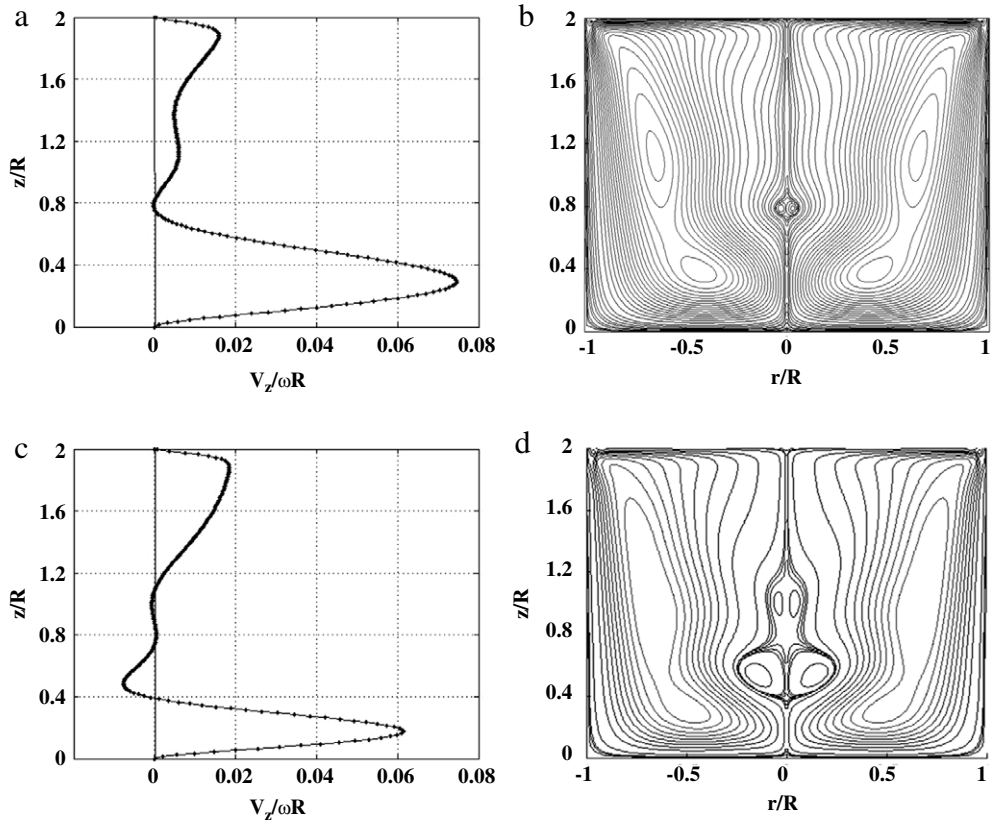

Fig. 6. Numerical results of the axial velocity at the cylinder axis (left) and equispaced streamlines (right) corresponding to the same situation of Fig. 3. (a),(b) One bubble is observed for $H/R = 2$ and $Re = 1474$. (c), (d) Two bubbles are observed for $H/R = 2$ and $Re = 1836$. In panels (b) and (d), 26 and 15 countours respectively are plotted. The curve of v_z at the axis allows us to determine precisely at which Re the onset of VB takes place and the localization of the stagnation point.

Table 1
Experimental and numerical critical Reynolds numbers corresponding to the appearance of the first VB for different aspect ratios without rod. The experimental values (1) were taken from [5] and the (2) were obtained in this work using the DPIV technique.

H/R	Exp. (1)	Exp. (2)	Num.
1.5	1068	1098	1095
2	1450	1474	1474
2.5	1910	1973	1935

Table 2
Experimental and numerical critical Reynolds numbers corresponding to the appearance of the first VB for different aspect ratios and radius of the rod.

H/R	$R_r/R = 0.0250$		$R_r/R = 0.0625$		$R_r/R = 0.1250$	
	Exp.	Num.	Exp.	Num.	Exp.	Num.
1.5	971	950	1036	1020	1246	1200
2	1313	1340	1431	1435	1671	1700
2.5	1785	1780	1887	1910	2187	2250

in these configurations. As in the case where no rod was used, the differences between numerical and experimental results are less than 2%. Thus, the DPIV technique provides an accurate method to determinate the onset of VB through the analysis of vertical velocity profiles.

The critical Reynolds number as a function of the radius of the rod is depicted in Fig. 7 and Table 2 for three different aspect ratios of the cylinder. Experimental and numerical results show an excellent agreement. According to these data, it must be concluded that for $R_r/R < 0.065$, the VB is anticipated, i.e. Re_c decreases with the presence of the rod; while for $R_r/R > 0.065$, the VB is delayed, i.e. Re_c is increased. Note that for $R_r/R \sim 0.065$, there are not significant difference between the critical Re numbers for the cases with or without rod.

In order to analyze the response of the system to larger radius of the rod, we also obtained numerically the Re_c for $R_r/R = 0.25$. In this case, the critical Reynolds number is increased approximately 65%. A clear modification is noted also in the vorticity structure, as can be seen from Fig. 8. It is worth mentioning that our numerical results for the vorticity in the absence of rods, panel (a), are in agreement with those given by Lopez [6]. In spite of the fact that the onset is anticipated for $R_r/R = 0.025$ (b) and delayed for $R_r/R = 0.0625$ (c) and $R_r/R = 0.125$ (d), the structure of the vorticity is similar in all the cases.

It is interesting to compare our results with those obtained by Husain et al. [13] and Mullin et al. [11], and emphasize the differences with our results. In these two works, it was suggested that a very slender rod at rest does not introduce significant changes in VB phenomena. In Ref. [11], the authors used an inner cylinder with ratio $R_r/R = 0.1$. They did not find qualitative effects on the appearance of stagnation points on the core of the induced vortex regardless of whether the inner cylinder is rotating or stationary. Following a different approach, in our experiments we observed appreciable changes in the critical value of Re as a function of the dimensionless radius R_r/R. It is worth mentioning that in Ref. [11] those critical values were not obtained and the radius was kept fixed. In addition, looking carefully at Fig. 3 of this reference, we observe slight differences between the experimental and the numerical results which, according to the authors, are a consequence of the difficulties to find a reliable experimental measure for the onset of VB. For this reason, we took specially careful measurements in the experimental setup with stationary rods. Afterwards, Husain et al. [13] contradicted some of the results of Mullin et al. showing that an adequate co- or counter-rotation of the inner cylindrical can be an effective means to either suppress

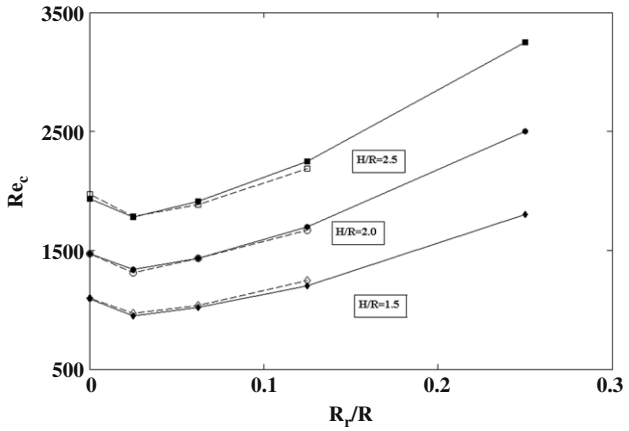

Fig. 7. Experimental (open symbols) and numerical (filled symbols) values of the critical Reynolds numbers corresponding to the appearance of the first bubble as a function of the rod radius, for different values of the aspect ratio $H/R = 1.5$ (diamonds), $H/R = 2.0$ (circles) and $H/R = 2.5$ (squares).

or enhance VB. They found, using visualization techniques, that the core of the VB has the same localization and size with and without rod for $R_r/R = 0.04$. Our results are in agreement with their about this point, but, in addition, our method allows us to accurately obtain the Re_c at the onset of VB.

At this point it is interesting to consider the origin of the effect of the rod on VB, and in particular if it is of viscous nature or not. Inviscid theory has largely been used to explain the origin of VB. The results has been sufficiently successful to support the belief that VB may occur with no presence of viscosity. However, the decrease of Re_c due to small rods ($R_r/R < 0.065$) appears to be of viscous origin. The presence of the rods tends to reduce the velocity of the fluid due to stress at the rod surface, favoring the appearance of the stagnation point and thus reducing the critical value Re_c needed for the appearance of VB. The reducing effect of the viscosity is also present in the absence of rods and may begin the process that leads to the formation of the stagnation point (as occur in pipe flows [7]), but the presence of the rigid limit imposed by the rod enhances this effect very much. Thus, a very thin rod produces an significant effect, because the boundary conditions at the axis changes drastically from free to no-slip. This produces an appreciable change in Re_c. In fact, the limit $R_r \to 0$ is singular. The Re_c without rod has a finite difference with the Re_c for any rod, no matter how small the rod it is. A similar result was obtained in previous works where it has been shown that even a thin wire may promote the formation of VB in delta wings [31].

We note that, in the opposite limit, when the radius of the rod R_r is sufficiently large, the critical value of Re increases with increasing R_r (see Fig. 7). This effect could possibly be of similar origin than that which appears in unconfined flows [32]. Then, when R_r increases, this effect of inviscid nature can compensate the viscous one and finally VB is displaced to higher values of Re.

5. Summary and conclusion

In this work, we studied the changes in VB phenomena that are produced when a rod is located at the axis of the cylinder container. The experiments shown that the rod may increase or decrease the critical Reynolds number for the emergence of VB.

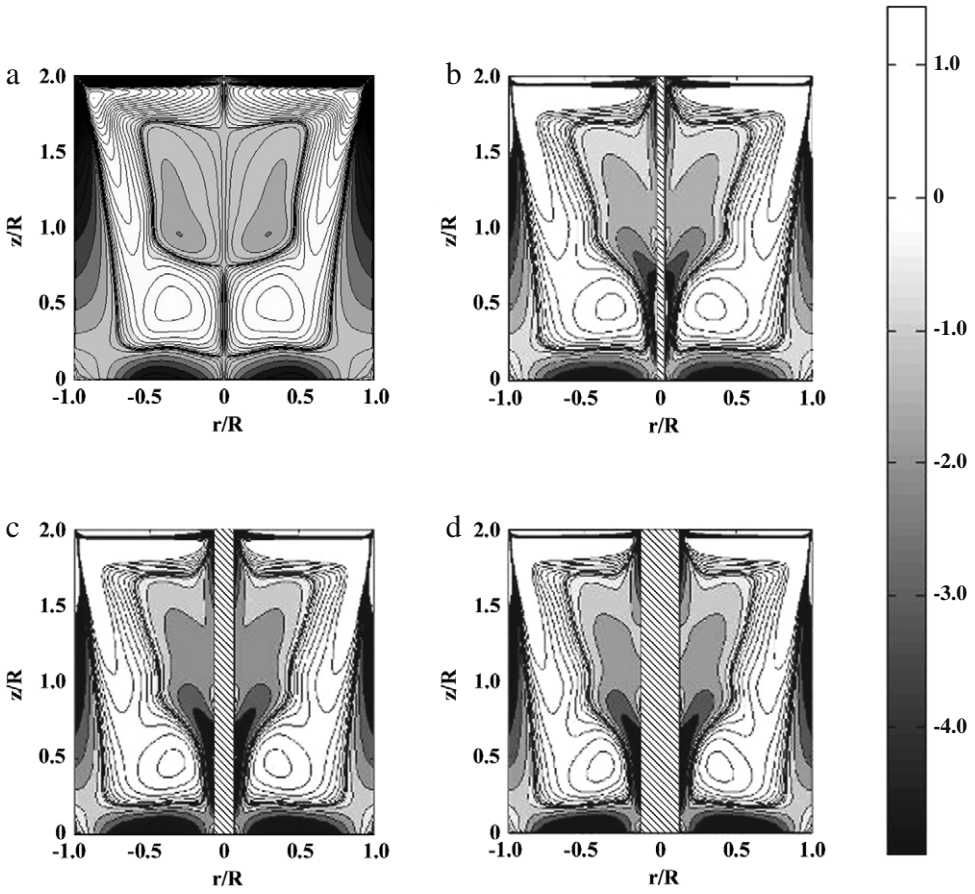

Fig. 8. Numerical results for the azimuthal component of the vorticity at the onset of VB and aspect ratio $H/R = 2$. The lined regions represent the stationary rod. (a) Without rod, $Re = 1474$. (b) Stationary rod of dimensionless radius $R_r/R = 0.025$ and $Re = 1340$. (c) Stationary rod with $R_r/R = 0.625$ and $Re = 1435$. (d) Stationary rod with $R_r/R = 0.125$ and $Re = 1700$. The scale, indicated in the colorbar at the right, is the same for all the panels.

The effect of small rods is to decrease Re_c, while Re_c is increased when R_r/R is beyond a certain critical value $(R_r/R)_c$, which is of order 0.065. This critical value depends weakly on the aspect ratio, decreasing smoothly with increasing H/R. The effects of the rods are of practical interest since may be used to perform a control of VB in a way that is simpler than other previously proposed in the literature, since it does not require additional auxiliary devices (in the sense that does not require the input of energy in order to move parts or to inject heat into the system as is the case of other methods). It is worth noting that this method, unlike the approach proposed in previous works, does not imply the addition of swirl near the axis. This simplicity is an interesting feature, making it more feasible to be used in engineering devices. The modification of the critical *Re* are very noticeable. For instance for the $R_r/R = 0.025$, the volume ratio (rod to cylinder) is $V_1/V_2 \sim 6 \times 10^{-4}$, while the decrease of the critical Reynolds number is about 10%. So that the shift of the critical Reynolds number is 20 times larger that the percent modification of the volume of the cylinder, showing the effectiveness of the method. The dependence of the critical *Re* with the rod diameter obtained experimentally is in very good agreement with that found with numerical calculations. We gave arguments to support that the enhancing effect of very small rods on VB is of viscous origin. Using a simple theoretical model for flow in pipes, we obtained that the influence of the inner cylinder on VB works in similar fashion in open flows, mainly for not too small values of $(R_r/R)_c$.

Acknowledgements

We acknowledge financial support from the Programa de Desarrollo de Ciencias Básicas (PEDECIBA, Uruguay) and Grants FCE 9028 and PDT54/037 (Conicyt, Uruguay).

References

[1] D.H. Peckham, S.A. Atkinson, Preliminary results of low speed wind tunnel tests on a gothic ratio 1.0, Aeronautical Research Council Report CP 508, 1957.
[2] H.U. Vogel, Experimentelle Ergebnisse ber die laminare Strmung in einem zylindrischen Gehuse mit darin rotierender Scheibe, MPI Bericht 6 (1968).
[3] S. Leibovich, The structure of vortex breakdown, Annu. Rev. Fluid Mech. 10 (1978) 221.
[4] S. Leibovich, Vortex stability and breakdown: Survey and extension, AIAA J. 22 (1984) 1192.
[5] M.P. Escudier, Observations of the flow produced in a cylindrical container by a rotating endwall, Exp. Fluids 2 (1984) 189.
[6] J.M. Lopez, Axisymmetric vortex breakdown. Part 1. Confined swirling flow, J. Fluid Mech. 221 (1990) 533.
[7] G.L. Brown, J.M. Lopez, Axisymmetric vortex breakdown. Part 2. Physical mechanisms, J. Fluid Mech. 221 (1990) 553.
[8] J.M. López, Unsteady swirling flow in an enclosed cylinder with reflectional symmetry, Phys. Fluids 7 (1995) 2700.
[9] J.M. López, Flow between a stationary and a rotating disk shrouded by a co-rotating cylinder, Phys. Fluids 8 (1996) 2605.
[10] Mark C. Thompson, K. Hourigan, The sensitivity of steady vortex breakdown bubbles in confined cylinder flows rotating lid misalignment, J. Fluid Mech. 496 (2003) 129.
[11] T. Mulin, J.S. Tavener, K.A. Cliffe, On the creation of stagnation points near straight and sloped walls, Phys. Fluids 12 (2000) 425.
[12] A. Mitchell, J. Delery, Research into vortex breakdown control, Progr. Aerospace Sci. 37 (2001) 385.
[13] Hyder S. Husain, Vladimir Shtern, Fazie Hussain, Control of vortex breakdown by addition of near-axis swirl, Phys. Fluids 15 (2003) 271.
[14] L. Mununga, K. Hourigan, M.C. Thompson, Confined flow vortex breakdown control using a small rotating disk, Phys. Fluids 16 (2004) 4750.
[15] K. Fujimura, H.S. Koyama, J.M. Hyun, A experimental study on vortex breakdown in a differentially-rotating cylindrical container, Exp. Fluids 36 (2004) 399.
[16] M. Piva, E. Meiburg, Steady axisymmetric flow in a open cylinder with a partially rotating bottom wall, Phys. Fluids 17 (2005) 063603.
[17] T.T. Lim, Y.D. Cui, On the generation of spiral-type vortex breakdown in an enclosed cylindrical container, Phys. Fluids 17 (2005) 044105.
[18] Z. Zhang, R.J. Hugo, Stereo particle image velocimetry applied to vortex breakdown, Exp. Fluids 40 (2006) 333.
[19] Peng Yu, Yan Zeng, Thong See Lee, Hong Tong Low, Steady axisymmetric flow in an enclosed conical frustum chamber with a rotating bottom wall, Phys. Fluids 20 (2008) 087103.
[20] Peng Yu, Thong See Lee, Yan Zeng, Hong Tong Low, Effects of conoidal lids on vortex breakdown in an enclosed cylindrical chamber, Phys. Fluids 18 (2006) 117101.
[21] P. Yu, T.S. Lee, Y. Zeng, H.T. Low, Characterization of flow behavior in an enclosed cylinder with a partially rotating end wall, Phys. Fluids 19 (2007) 057104.
[22] M.A. Herrada, V. Shtern, Vortex breakdown control by adding near-axis swirl and temperature gradients, Phys. Rev. E 68 (2003) 041202.
[23] D. Lo Jacono, J.N. Srensen, M.C. Thompson, K. Hourigan, Control of vortex breakdown in a closed cylinder with a small rotating rod, J. Fluids Struct. 24 (2008) 1278.
[24] J.M. Lopez, Y.D. Cui, F. Marques, T.T. Lim, Quenching of vortex breakdown oscillations via harmonic modulation, J. Fluid Mech. 599 (2008) 441.
[25] R.J. Adrian, Particle-imaging techniques for experimental fluid mechanics, Ann. Rev. Fluid Mech. 23 (1991) 261–304.
[26] J. Westerweel, Fundamentals of digital particle image velocimetry, Meas. Sci. Technol. 8 (1997) 1379–1392.
[27] J. Ferziger, M. Peric, Computational Methods for Fluid Dynamics, Springer-Verlag, 2002.
[28] G. Usera, A. Vernet, J.A. Ferré, Use of Time resolved PIV for validating LES/DNS of the turbulent flow within a PCB enclosure mod, Flow. Turb. Comb. 77 (2006) 77–95.
[29] G. Usera, A. Vernet, J.A. Ferré, A parallel block-structured finite volume method for flows in complex geometry with sliding interfaces, Flow. Turb. Comb. 81 (2008) 471–495.
[30] G. Usera, IMFIA, Facultad de Ingeniería, J.H. Reissig 565, CP:11.300, Montevideo, Uruguay. The code is freely available for academic use through the web site (www.fing.edu.uy/imfia/caffa3d.MB) as of May, 2009.
[31] H. Akilli, B. Sahin, D. Rockwell, Control of vortex breakdown by a coaxial wire, Phys. Fluids 15 (2003) 123.
[32] G.K. Batchelor, An Introduction to Fluid Dynamics, Cambridge University Press, Cambridge, 1967.